Particle production in a bouncing universe

Mustafa Saeed,[1,*] Irfan Javed,[2,†] and Aiman Nauman[3,‡]

[1]*Centre College, Danville, KY, USA 40422*

[2]*Department of Mathematics and Statistics, University of New Brunswick, Fredericton, NB, Canada E3B 5A3*

[3]*Mathematical Institute, University of Oxford, Oxford, OX2 6GG, UK*

In massless scalar field cosmology, imposing the universe's physical volume as fundamentally discrete resolves the big bang singularity via a big bounce. We use quantum field theory on curved background to numerically track the number of particles created in the vacuum of a quantum field that propagates through the cosmological bounce. We find that due to geometry's evolution, particle production in all modes initially rises, sharply peaks at the bounce, and varies slowly afterwards. Further, by comparing with the case of a quantum field propagating on an expanding universe, we discover that the bouncing universe's imprints on quantum matter are distinct: notably, the late time particle production across modes resembles a thermal spectrum. We then use semiclassical gravity and find similar qualitative results. Here, we also determine how particle production affects geometry's evolution. Our study adds to existing literature on gravity-matter interactions in the context of a bouncing universe, contributes to searches of a bouncing universe's signatures, and strengthens the link between gravity and thermodynamics.

I. INTRODUCTION

General relativity (GR)—a theory of classical spacetime, matter, and their interactions—enables investigations of black holes and the expanding universe [1]. However, GR is not a microscopic theory and is inapplicable at singularities, such as the end point of gravitational collapse of sufficiently massive matter configurations and the cosmological big bang. It is expected that these singularities will be resolved by quantum effects.

These depend on the quantization as different schemes are inequivalent [2]. For example, Schrödinger and polymer quantizations use for their configuration spaces the $\mathbb{R}^n$ and a lattice, respectively. The two schemes lead to different results, when applied to simple systems such as the harmonic oscillator [3] for example.

The study of quantum matter on a fixed curved geometry is called quantum field theory on curved background (QFTCB) [4, 5]. A notable result due to QFTCB is that the expansion of the universe creates energy excitations—called particles—in the field vacuum [5], a finding which is used to probe physics beyond the standard model, dark matter, and cosmological perturbations [6]. Another finding due to QFTCB is that a black hole radiates like a hot blackbody [7]. Similar to thermal energy's being the motion of microscopic particles, a black hole's temperature hints at an underlying microscopic structure.

The formalism that describes the consistent joint propagation of classical geometry and quantum matter is called semiclassical gravity (SG) [8]; its difference from QFTCB lies in that quantum matter is now allowed to backreact on curved geometry, meaning that the latter is no longer fixed as in QFTCB. In one version of canonical SG, the gravity phase space variables and matter quantum state are the relevant degrees of freedom that evolve via a state-dependent Hamiltonian constraint and the time-dependent Schrödinger equation, respectively [9–11]. Application of this SG approach to cosmology has demonstrated how particle production modifies the evolution of classical geometry [10].

Quantum geometry, quantum matter, and their interactions are described by quantum gravity (QG) [12–14]. The resolution of singularities and explanation of gravity's thermodynamic properties are some of QG's goals. There are many QG approaches. For instance, nonperturbative canonical QG is described in connection-triad terms. The latter—called loop quantum gravity (LQG)—mirrors the quantization of the electromagnetic, weak, and strong interactions. Therefore, in LQG, gravity is expressed in connection-triad variables before it is quantized using a scheme that incorporates discreteness [15, 16].

LQG motivates loop quantum cosmology (LQC), in which homogeneity and isotropy is imposed on classical gravity expressed in connectrion-triad variables before quantization. A notable finding of LQC is the resolution of the big bang singularity via the big bounce [17, 18]. The big bounce is also found in effective LQC, which is classical cosmology expressed in connection-triad variables with LQC corrections [19, 20].

However, this result is not exclusive to effective LQC. Classical cosmology expressed in metric variables including polymer quantum effects also resolves the big bang singularity via the big bounce [21, 22]. This indicates that the resolution of the big bang singularity follows not

*Electronic address: mustafa.saeed@centre.edu
†Electronic address: i.javed@unb.ca
‡Electronic address: aiman.nauman@lmh.ox.ac.uk

from a choice of variables but from a quantization scheme that incorporates discreteness. Bouncing cosmologies are also arrived at in other formalisms such as higher-order gravity theories and other QG approaches, such as string gas cosmology; see [23] for a review.

Given that the bouncing universe is an outcome of the resolution of the big bang, it is important to search for its signatures just as we look for the signatures of the big bang, in the cosmic microwave background (CMB) for example. Work in this direction mostly includes cosmological perturbation theory, in which inflation is preceded by a bounce and a phase of contraction instead of the big bang. Here, the evolution of perturbations across the additional contracting and bouncing phases leads to findings different from those of standard inflation that can be verified via the cosmic microwave background (CMB) data [24–27]. A different work proposes dark matter production through the bounce as a means to detect the the bouncing universe's signatures [28]. Another uses the Unruh-DeWitt detector to compare the total particles produced in the vacuum of a conformally coupled massless scalar field in the expanding universe due to GR and the post-bounce universe due to effective LQC [29].

With a similar motivation of studying gravity-matter interactions in the context of a bouncing universe and identifying its signatures, we numerically study particle production in the vacuum of a massless scalar field that propagates through the bounce using QFTCB and SG. Our work is different from the existing literature on the subject in several aspects. First, we study particle production in a scalar field that propagates through the universe's contracting, bouncing, and expanding phases, not just the post-bounce expansion phase, and secondly, we look at particle production in the vacua of individual field modes. Notably, these extend the work in [29]. Lastly, we generalize to SG to explore how the results differ and also to determine the effect of particle production on the effective geometry's evolution; this direction does not exist in the literature to the best of our knowledge.

Using QFTCB, we find that particle production in all modes initially rises, sharply peaks at the bounce, and varies slowly afterwards. At late times, we compare particles produced across modes with corresponding results for a scalar field that propagates on an expanding universe. In the case of an expanding universe, we find that the most particles are produced in the lightest mode. This is aligned with the intuition that lighter modes are easier to excite. For the bouncing universe, given that the field evolves for an equal time pre- and post-bounce, we find that the late-time particle production across modes resembles a thermal spectrum with the most particles produced in an intermediate mode. Upon generalizing the formalism to SG, we find similar features for particle production and also demonstrate how the quantum matter modifies the effective geometry. These results contribute to searches of the bouncing universe's signatures, strengthen links between gravity and thermodynamics, and provide an example of how quantum matter affects effective geometry.

What follows is a review of effective cosmology in Sec. II, study of a quantum field on this effective background using QFTCB and SG in Sec. III, and some reflections on the results in Sec. IV. Details for Sec. II appear in [22] and those for Sec. III in AN's thesis.

II. A BOUNCING UNIVERSE

We consider massless scalar field cosmology with metric

$$ds^2 = -N(t)^2 dt^2 + v(t)^{\frac{2}{3}} \left(dx^2 + dy^2 + dz^2\right), \qquad (1)$$

where $v(t)$ is the cube of the scale factor, and scalar field $\phi(t)$. The canonical action is

$$S = V_0 \int dt \left[\left(\frac{1}{16\pi G}\right) \dot{v} p_v + \dot{\phi} p_\phi - N\mathcal{H}\right]. \qquad (2)$$

Here, V_0 is the volume of the cubical fiducial cell,

$$V_0 = \int d^3x, \qquad (3)$$

that the calculations are restricted to; overdots indicate derivatives with respect to coordinate time; p_v and p_ϕ are the gravity and scalar field momenta, respectively; N is the lapse; and $\mathcal{H}$ is the Hamiltonian constraint:

$$\mathcal{H} \approx 0, \qquad \mathcal{H} = -\left(\frac{1}{16\pi G}\right)\left(\frac{3\, v\, {p_v}^2}{8}\right) + \frac{{p_\phi}^2}{2v}. \qquad (4)$$

While fundamental Poisson brackets,

$$\{v, p_v\} = \frac{16\pi G}{V_0} \quad \text{and} \quad \{\phi, p_\phi\} = \frac{1}{V_0}, \qquad (5)$$

depend on the fiducial volume, the classical equations of motion do not. These and the Hamiltonian constraint (4) lead to the Friedmann equation (note that N has been set to 1 here)

$$H^2 = \frac{8\pi G}{3}\rho, \qquad (6)$$

where the Hubble parameter and the field's energy density are

$$H = \frac{\dot{v}}{3v} \quad \text{and} \quad \rho = \frac{p_\phi^2}{2v^2}, \qquad (7)$$

respectively. The Friedmann equation leads to an expanding (contracting) universe, which begins (ends) with a big bang (crunch); properties of each will be discussed shortly.

This classical theory is expressed in terms of scale-dependent variables. Under the rescaling of the coordinates

$$t \to t, \qquad x \to lx, \qquad (8)$$

where l is a dimensionless constant, and the condition that the metric and action do not scale, the parameters and degrees of freedom in the theory rescale as

$$\begin{aligned} &V_0 \to l^3\, V_0, \quad N\ (=1) \to N, \quad v \to l^{-3}\, v, \\ &p_v \to p_v, \quad \phi \to \phi, \quad p_\phi \to l^{-3}\, p_\phi. \end{aligned} \tag{9}$$

Due to their applicability across scales, we use the above relations to construct scale-invariant variables—such as $V_0 v$—to express the theory with.

Additionally, to simplify future simulations, we express the theory in terms of dimensionless coordinates, parameters, and variables. In natural units, $\hbar = c = 1$, the action is dimensionless, and the terms appearing in the theory have the following dimensions of length L:

$$\begin{aligned} &V_0 = L^3, \quad x = t = L, \quad N = v = 1, \\ &\phi = p_v = L^{-1}, \quad p_\phi = L^{-2}. \end{aligned} \tag{10}$$

To make the theory dimensionless, all lengths must be expressed as dimensionless multiples of the Planck length l_P using Newton's constant via

$$\sqrt{G} = l_P. \tag{11}$$

For example, $G^{-3/2} V_0 v$ is dimensionless.

Using the scaling relations and appropriate dimensional assignments, one can define scale-invariant dimensionless quantities to express the theory with. The dimensionless time is $\bar{t} = G^{-1/2}\, t$, and the new canonical degrees of freedom are

$$\begin{aligned} \bar{v} &= \left(\frac{V_0}{16\pi}\right)\left(\frac{1}{\sqrt{G}}\right)^3 v, \qquad p_{\bar{v}} = \sqrt{G}\, p_v, \\ \bar{\phi} &= \sqrt{16\pi G}\, \phi, \qquad\qquad p_{\bar{\phi}} = \left(\frac{V_0}{\sqrt{16\pi G}}\right) p_\phi. \end{aligned} \tag{12}$$

Factors of 16π are included in these definitions for simplicity. We are thus led to the action

$$S = \int d\bar{t}\, \left(\frac{d\bar{v}}{d\bar{t}}\, p_{\bar{v}} + \frac{d\bar{\phi}}{d\bar{t}}\, p_{\bar{\phi}} - \bar{\mathcal{H}}\right), \tag{13}$$

where the Hamiltonian is

$$\bar{\mathcal{H}} = -\left(\frac{3\, \bar{v}\, {p_{\bar{v}}}^2}{8}\right) + \frac{{p_{\bar{\phi}}}^2}{2\bar{v}}. \tag{14}$$

Hereon, the overbars will be dropped and overdots will indicate time derivatives with respect to dimensionless time. The Hamiltonian (14) and the equations of motion lead to the Friedmann equation

$$H^2 = \frac{\rho}{6}. \tag{15}$$

The solution is

$$v = \pm \frac{\sqrt{27t^2}}{6}\, \tilde{p}_\phi, \tag{16}$$

where $\tilde{p}_\phi$ is a constant of motion and the positive (negative) solution represents an expanding (contracting) universe defined for $t \in \mathbb{R}^{+(-)}$ with $t = 0$ representing the big bang (crunch).

To arrive at the bounce, it is sufficient to include quantum discreteness corrections to the universe's volume. This can be achieved by polymer quantizing gravity variables via a volume lattice with discretization λ. We then pick a semiclassical state peaked at the classical phase space variables to calculate the expectation value of the Hamiltonian operator. Taking the limit that the state is sharply peaked, we get the effective Hamiltonian

$$\mathcal{H}_e = -\left(\frac{3}{8}\right) v\, \left[\frac{\sin(p_v\, \lambda/2)}{\lambda/2}\right]^2 + \frac{{p_\phi}^2}{2v}, \tag{17}$$

which leads to the effective Friedmann equation

$$H^2 = \frac{\rho}{6}\left(1 - \frac{\rho}{\rho_c}\right), \quad \rho_c = \frac{3}{8\lambda^2}. \tag{18}$$

This indicates that the universe bounces when $\rho = \rho_c$. The solution is

$$v = \frac{\sqrt{27t^2 + 48\lambda^2}}{6}\, \tilde{p}_\phi, \tag{19}$$

where $\tilde{p}_\phi$ is a constant of motion.

III. PARTICLE PRODUCTION IN COSMOLOGY

In this section, we use QFTCB to study particle production in the vacuum of a massless inhomogeneous scalar field that propagates on a cosmological background. We determine if a bouncing universe's imprint on quantum matter is distinct by comparing particle production in contracting, expanding, and bouncing universes. Then, we use SG to jointly evolve geometry and quantum matter and study how the results differ.

A. Quantum field on a cosmological background

1. Formalism

An inhomogeneous massless scalar field on an FLRW background described by the metric with $N = 1$ has the following Hamiltonian in spatial Fourier space:

$$\begin{aligned} \mathcal{H}_\phi &= \int \frac{d^3k}{(2\pi)^3}\left(\frac{1}{2}\right)\left[\frac{p_k^2}{v} + v\left(\frac{k}{v^{\frac{1}{3}}}\right)\phi_k^2\right] \\ &\equiv \int \frac{d^3k}{(2\pi)^3}\, h_k. \end{aligned} \tag{20}$$

Here, $k = |\vec{k}|$ and (ϕ_k, p_k) are the spatial Fourier transforms of the scalar field phase space variables. Notably, the field modes decouple and each mode—regardless of its characteristic wavelength $L_k = k^{-1}$—resembles an oscillator with a time-dependent mass $m = v$ and frequency $\omega = k\,v^{-\frac{1}{3}}$. Further, the Hubble scale $L_H = 3v^{\frac{2}{3}}\dot{v}^{-1}$ does not appear in the potential term. For these reasons, each field mode is quantized as an oscillator.

The state for each mode is chosen to be the Gaussian

$$\psi_k\left(\phi_k, t\right) = \beta_k(t) \exp\left[-\alpha_k(t)\phi_k^2\right], \tag{21}$$

where $\alpha_k(t)$ and $\beta_k(t)$ are time-dependent complex numbers. The normalization condition gives

$$|\beta_k|^2 = \sqrt{\frac{2\mathrm{Re}(\alpha_k)}{\pi}}. \tag{22}$$

For evolution, we substitute this Gaussian ansatz in the time-dependent Schrödinger equation

$$i\dot{\psi}_k = \hat{h}_k\psi_k, \tag{23}$$

which leads to

$$\begin{aligned} i\dot{\alpha} &= \frac{1}{2v}\left(4\alpha_k^2 - v^{\frac{4}{3}}k^2\right), \\ i\frac{\dot{\beta}_k}{\beta_k} &= \frac{\alpha_k}{v}. \end{aligned} \tag{24}$$

We initialize each mode at $t = t_0$ in its Hamiltonian's instantaneous ground state. To set these initial conditions, we compare 21 with the ground state of an oscillator,

$$\psi(x) = \left(\frac{mw}{\pi}\right)^{\frac{1}{4}} \exp\left(-\frac{mw}{2}x^2\right), \tag{25}$$

and use the correspondences $m = v$ and $\omega = kv^{-\frac{1}{3}}$ to fix

$$\alpha_k(t_0) = \frac{kv(t_0)}{2}, \quad \beta_k(t_0) = \left(\frac{kv(t_0)}{\pi}\right)^{\frac{1}{4}}. \tag{26}$$

We re-emphasize that this is possible because the Hamiltonian for each mode (20)—regardless of the Hubble scale and its characteristic wavelength—resembles that of a harmonic oscillator with time-dependent mass and frequency.

To compute particle production at a later time $T \geq t_0$, the Hamiltonian's instantaneous eigenstates $\psi_k^n(t)$ are required. These are computed from the eigenstates at time $t = t_0$ via the adiabatic approximation for simplicity. Then, average particle number in ψ_k at time $t = T$ is

$$\langle \hat{n}_k(T)\rangle = \sum_{n_k=0}^{\infty} n_k \,|\, \langle\, \psi_k^n(T) \,|\, \psi_k(T)\, \rangle\, |^2, \tag{27}$$

which evaluates to

$$\langle \hat{n}_k \rangle = \frac{|z_k|^2}{1 - |z_k|^2} \tag{28}$$

with

$$z_k = \frac{v^{\frac{2}{3}}k - 2\alpha_k}{v^{\frac{2}{3}}k + 2\alpha_k}; \tag{29}$$

see [10, 30, 31] for details. As expected, at $t = 0$,

$$\langle \hat{n}_k \rangle = 0. \tag{30}$$

Using this proposal, cosmological particle production in the vacuum of a quantum field can be computed at all times. We will apply this to the contracting and expanding universes described by (16) in addition to the bouncing universe given by (19). (We set $\tilde{p}_\phi$ equal to 1 in the simulations.)

2. Results

For the contracting universe, we performed the simulation from $t = -\tau$ through $t = -t_P$, where $\tau = 500$ and t_P is the Planck time, with a time step of $\Delta t = 0.5$ (the results do not change with lower step sizes). The results are in the left column in Fig. 1. The top subfigure shows the contracting universe, the central one compares the Hubble scale with the comoving wavelengths of some modes, and the bottom one displays particle production in these modes. We note that particle production occurs in all modes. Specifically, it rises sharply after initialization and when the curvature reaches a maximum. Further, the number of particles at late times is larger for lighter modes. These results are aligned with the intuition that a varying geometry creates particles and that the lighter modes are easier to excite. This trend is more apparent in the left column in Fig. 2, which is particle production spectrum across 10^3 modes at $t = 500$.

For the expanding universe, we performed the simulation from $t = t_P$ till $t = \tau$ with time step $\Delta t = 0.5$. The results are in the central column in Fig. 1. As before, the top subfigure is a plot of the geometry, the central one compares the Hubble scale with the comoving wavelengths of some modes, and the bottom one displays particle production in these modes. Here too, particle production occurs in all modes; more precisely, it rises sharply after initialization and varies steadily afterwards. The rise is sharper compared to the previous case because the field experiences high curvature in the beginning. However, the late time particle production spectrum is identical.

For a bouncing universe, we performed the simulation from $t = -\tau$ till $t = \tau$ with $\Delta t = 0.5$. The results are in the right column of Fig. 1. The top subfigure displays the evolution of volume. The central one, which compares the Hubble scale with the comoving wavelengths of some modes, shows that all modes enter the Hubble horizon at the bounce, a feature that was absent in the case of the contracting and expanding universes. Another new feature is that some modes—like the green and yellow ones—start inside the horizon, exit it during

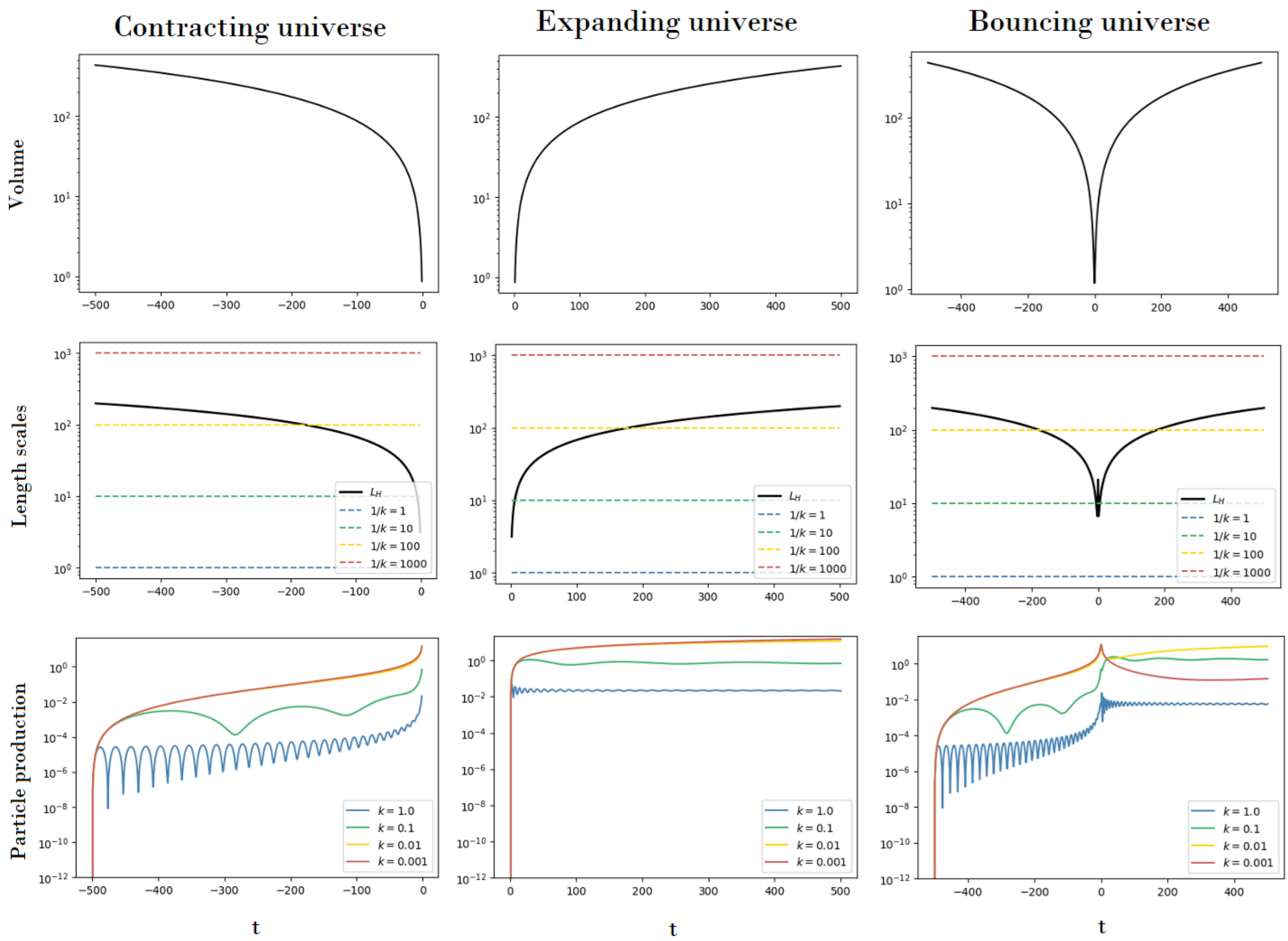

FIG. 1: Particle production in the contracting, expanding and bouncing universes

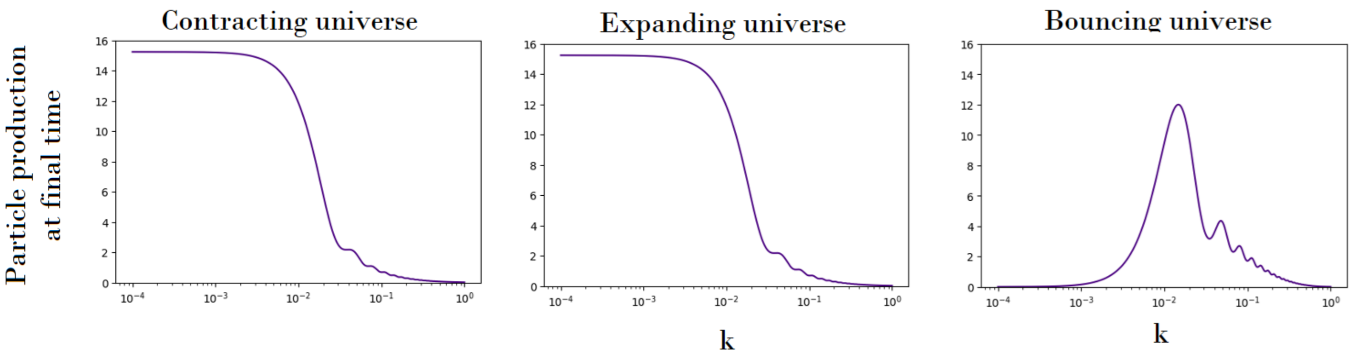

FIG. 2: Late time particle production spectrum

the contracting phase, and re-enter during the expanding phase.

The bottom subfigure shows particle production in the selected modes. It indicates that particle production initially rises, sharply peaks at the bounce, and then varies steadily. Notably, the number of particles for $k = 0.001$ is lesser than that for $k = 0.01$ despite the former's being the lighter mode. This trend is apparent in the right column of Fig. 2, which shows the particle production spectrum across 10^3 modes at $t = 500$. It is qualitatively different from those of the contracting and expanding universes. Specifically, the spectrum shows suppression of the lighter and heavier modes (in terms of particle production) with a peak in the middle.

We also observe that this spectrum resembles a Planckian blackbody spectrum. In terms of wavenumber, the spectral energy density is

$$u_{A,T}(k) = \frac{16\pi A\, k^3}{e^{\frac{2\pi k}{T}} - 1},$$

where T is temperature and A is an overall normalization. We note that the precise normalization in the Planck formula comes about from the detailed analysis in the context of a black body to give the energy emitted per unit time per unit solid angle per unit frequency; since we do not perform the detailed calculation for our spectrum, we allow for the normalization parameter A in fitting rather than having the only parameter T as in Planck's formula. The result of fitting Planck's formula to our spectrum is shown in Fig. 3; the parameter values turn out to be $A \approx 9.5 \times 10^5$ and $T \approx 3.4 \times 10^{-2}$ with least-squares regression coefficient $R^2 \approx 0.90$.

The spectra for different λ are shown in Fig. 4. Notably, more particles are produced for smaller λ. This is in line with the intuition that smaller λ implies smaller volume and higher curvature at the bounce, which produces more particles.

3. *Other bouncing universes*

Using QFTCB, we also study particle production due to other bouncing universes described by an engineered $v(t)$. The selected $v(t)$ are not found by solving Einstein's equations for some matter type. They are useful because they allow us to probe the properties of the spectrum further. The cases we explored are represented by the following.

$$\begin{aligned}
\text{Single Gaussian bounce I:} \quad & v(t) = \bar{v} - (\bar{v} - v_c)\, \exp\left(-\frac{t^2}{2\,(\sigma\tau)^2}\right), \\
\text{Single Gaussian bounce II:} \quad & v(t) = \bar{v} + (\bar{v} - v_c)\, \exp\left(-\frac{t^2}{2\,(\sigma\tau)^2}\right), \\
\text{Single quadratic bounce I:} \quad & v(t) = (\bar{v} - v_c)\left(\frac{t}{\tau}\right)^2 + v_c, \\
\text{Single quadratic bounce II:} \quad & v(t) = (v_c - \bar{v})\left(\frac{t}{\tau}\right)^2 + 2\bar{v} - v_c, \\
\text{Two sinusoidal bounces I:} \quad & v(t) = (\bar{v} - v_c)\sin\left(\frac{\pi t}{\tau}\right) + \bar{v}, \\
\text{Two sinusoidal bounces II:} \quad & v(t) = (v_c - \bar{v})\sin\left(\frac{\pi t}{\tau}\right) + \bar{v}.
\end{aligned}$$

Here, the universes evolve from $t = -\tau$ till $t = \tau$, $\bar{v}$ is the initial and final volume for all universes, v_c is the critical Planckian volume, and σ controls the width of the Gaussian bounces. We choose $\sigma = 1/4$ to ensure that $v(t = \pm\tau) \approx \bar{v}$. The universes labeled I initially contract and bounce at critical volume v_c, after which they expand. While the Gaussian and quadratic universes return to $\bar{v}$ after a single bounce, the sinusoidal one undergoes an additional bounce at $2\bar{v} - v_c$ before returning to $\bar{v}$. The universes labeled II initially expand and bounce at large volume $2\bar{v} - v_c$, after which they contract. Just as in the case of the universes labeled I, the Gaussian and quadratic universes return to $\bar{v}$ after a single bounce whereas the sinusoidal one does the same after undergoing an additional bounce at v_c.

To compare with the effective universe results from before, we choose the same τ and $\bar{v}$. The results are in Fig. 5. Note that a spectrum like the bouncing universe's from Fig. 2 is also present for the Gaussian II and Quadratic II universes that expand and then contract. This suggests that a condition for such a spectrum to be produced might be that $|\dot{v}|$ decreases to zero and then increases; alternatively, the comoving Hubble scale decreases, becomes infinite, and then increases. Relatedly, the spectrum is not due to the field experiencing high curvature. Curvature affects only the peak on the spectrum. This is shown via comparisons of Gaussian I with II and Quadratic I with II: the latters have much lesser particle production due to the field's experiencing a lower overall curvature. Further verification comes from the case of multiple bounces—compare Sinusoidal I with II. These have a high and low curvature bounce. It appears that the net number of particles produced is similar in both because the field in both cases experiences

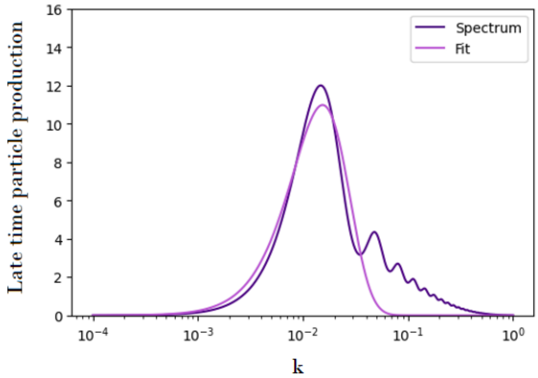

FIG. 3: Late time particle production spectrum

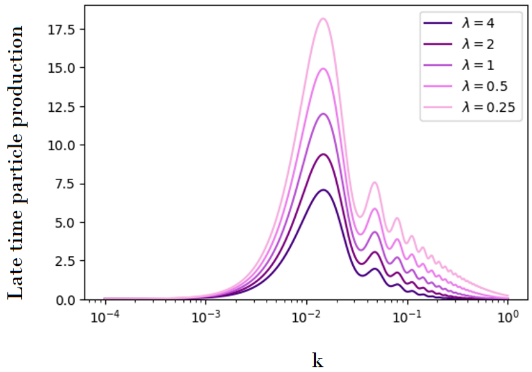

FIG. 4: Late time particle production spectrum for different polymer scales λ

the same curvature overall no matter whether it sees expansion or contraction first (equivalently, a low or high curvature first).

B. Semiclassical cosmology

1. Formalism

A system of effective cosmological geometry and massless (classical) homogeneous scalar field has Hamiltonian constraint (17), which leads to the effective Friedmann equation (18). Our semiclassical cosmological model comprises the polymer quantum corrected geometry and a quantum massless inhomogeneous scalar field. The system has the state-dependent effective Hamiltonian constraint

$$\mathcal{H}_{e,\psi} = -\left(\frac{3}{8}\right) v \left[\frac{\sin(p_v\,\lambda/2)}{\lambda/2}\right]^2 + v\,\langle\hat{\rho}\rangle_\psi, \tag{31}$$

where

$$\hat{\rho} = \frac{1}{v}\int \frac{d^3k}{(2\pi)^3}\left(\frac{1}{2}\right)\left[\frac{\hat{p}_k^2}{v} + v\left(\frac{k}{v^{\frac{1}{3}}}\right)\hat{\phi}_k^2\right] \tag{32}$$

$$\equiv \frac{1}{v}\int \frac{d^3k}{(2\pi)^3}\,\hat{h}_k. \tag{33}$$

The geometric phase space variables and matter state evolve via Hamilton's equations and the time-dependent Schrödinger equation, respectively:

$$\dot{v} = \{v, \mathcal{H}_{e,\psi}\}, \quad \dot{p}_v = \{p_v, \mathcal{H}_{e,\psi}\}, \quad i\dot{\psi}_k = \hat{h}_k\psi_k. \tag{34}$$

These preserve the Hamiltonian constraint under evolution:

$$\dot{\mathcal{H}}_e = 0. \tag{35}$$

The Hamiltonian constraint and the system of equations are equivalent to the effective Friedmann equation

$$H^2 = \frac{\langle\hat{\rho}\rangle_\psi}{6}\left(1 - \frac{\langle\hat{\rho}\rangle_\psi}{\rho_c}\right) \tag{36}$$

and the time-dependent Schrödinger equation. Initial data $\{v(t_0), \psi_k(t_0)\}$ are used to compute $\langle\hat{\rho}\rangle_\psi$. Then, the coupled first-order equations are solved for v and ψ_k at the next time step, and the process is repeated.

For the Gaussian ansatz (21),

$$\langle\rho\rangle_\Psi = \frac{1}{v}\int \frac{d^3k}{(2\pi)^3}\frac{1}{2\mathrm{Re}(\alpha_k)}\left[\frac{v}{4}\left(\frac{k^2}{v^{\frac{2}{3}}}\right) + \frac{|\alpha_k|^2}{v}\right], \tag{37}$$

and the time-dependent Schrödinger equation leads to (24). Therefore, it is sufficient to use (36) with (37) and

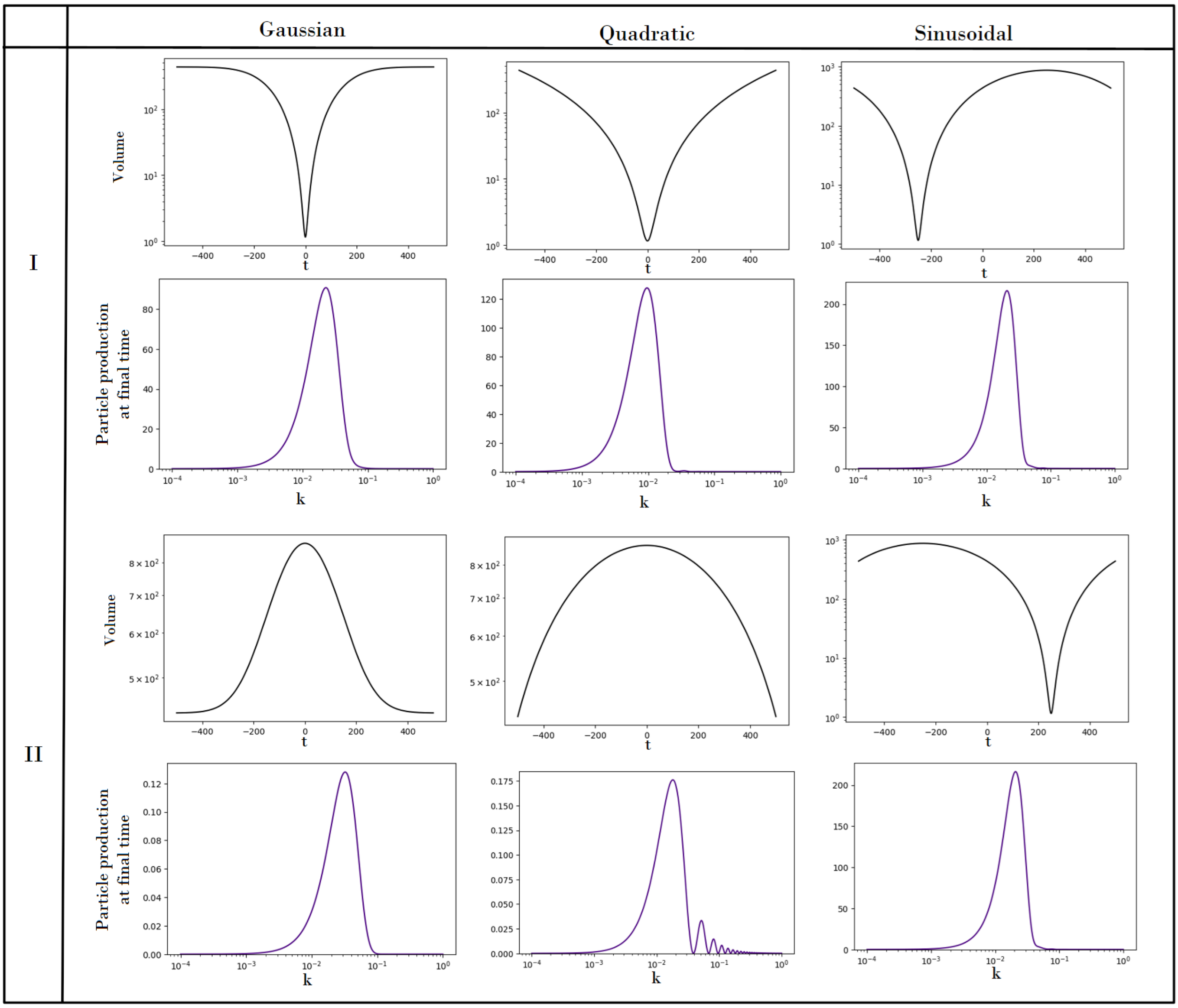

FIG. 5: Late time particle production spectrum for different bouncing universes

(24) to evolve v and α_k respectively. This joint evolution of effective geometry and quantum matter captures how geometry produces particles and how particle production affects the geometry.

2. Results

For simulations, we used $\lambda = 1$ and replaced the integral by a sum with 10^3 equispaced k-values between 0 and 1 on the log scale, the latter being a UV cutoff. We chose the log scale due to its utility in presenting the spectrum graphs; we also determined that this selection leads to similar results as choosing equispaced k on the standard scale.

At the starting time $t = -\tau$ with $\tau = 500$, the initial data were $\{v_0, \psi_k^0\}$, where v_0 is evaluated via (19). We used the negative root of (36) for evolution till $\langle\hat{\rho}\rangle_\psi = \rho_c$. This is the bounce, after which we used the positive root of (36). To compare with the QFTCB case, we performed the simulation for equal contraction and expansion times.

The results are in Fig. 6. The joint evolution of quantum matter and effective geometry causes a bounce that occurs later. Further, particle production in the selected modes is qualitatively similar to the QFTCB case. Some differences include more rapid oscillations in time and the larger number of particles produced overall. The late-time particle production spectrum in Fig. 7 shows similar features as the QFTCB case with some differences being no oscillations for the heavier modes and the larger number of overall particle production. The fit with the same density formula as before reveals $A \approx 6.6 \times 10^8$ and

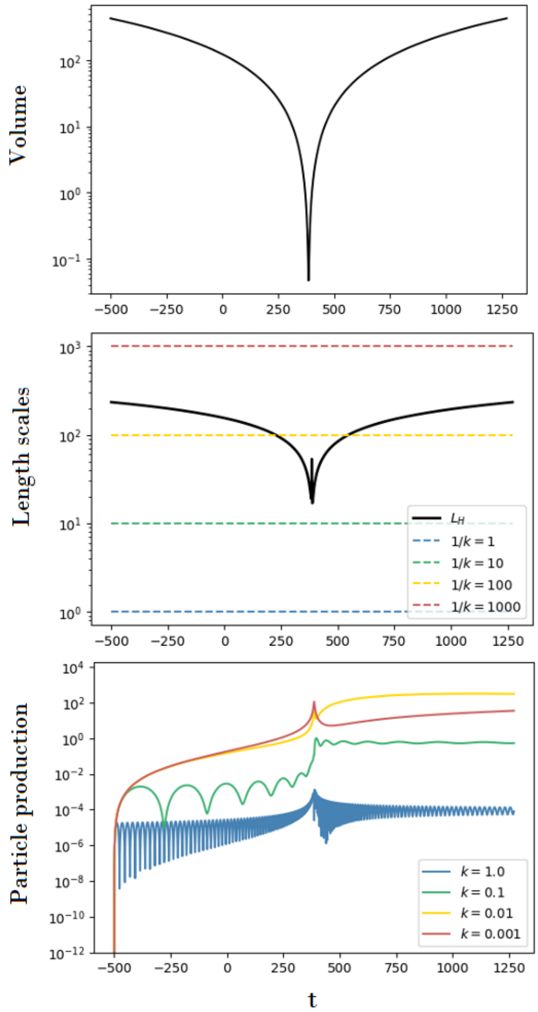

FIG. 6: Particle production through a cosmological bounce in semiclassical gravity

$T \approx 1.3 \times 10^{-2}$ with $R^2 \approx 0.97$. The lowering of the T and the increase in A correspond to the shifting of the peak to lower k values and greater overall particle production, respectively. The spectrum graphs for different polymer scales are in 8; these show that more particles are produced for a universe that attains a smaller critical volume—and a higher curvature—at the bounce.

IV. REFLECTIONS

A resolution of the big bang singularity comes from including quantum discreteness in the universe's volume, the classical geometric configuration. The resultant effective theory replaces the big bang singularity by a big bounce. We studied particle production in a quantum scalar field as it propagates across the cosmological bounce using QFTCB and SG with a goal of identifying the bounce's signatures.

The proposed formalism for QFTCB used the Schrödinger picture, whereby the state for each field mode was evolved by its time-dependent Hamiltonian. Using this formalism, we numerically tracked particle production through the contraction, bounce, and expansion phases of the universe. For SG, we additionally used a state-dependent Hamiltonian constraint and the Schrödinger equation for each field mode to jointly evolve the effective geometry and quantum matter, respectively. With this SG proposal, we studied how particle production and effective geometry influence each other.

Our results show that particle production in a bouncing universe is distinct from that in one that only expands or contracts. Moreover, the particle production across modes at late times resembles a thermal spectrum, for which we determined an approximate temperature. With SG, we also found that geometry's evolution is different from the case where there is no backreaction from matter. Therefore, this study adds to the existing literature on gravity-matter interactions in the context of a bouncing universe, contributes to searches for the bounce's signatures, and strengthens the link between gravity and thermodynamics.

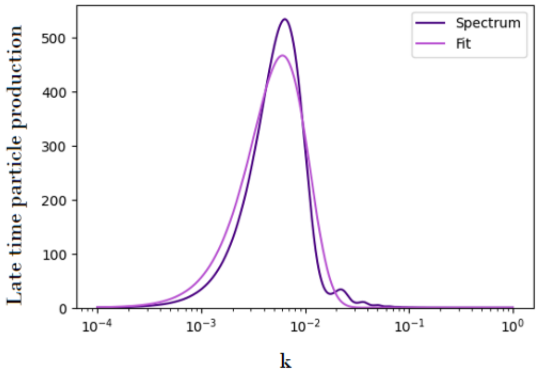

FIG. 7: Late time spectrum graph in semiclassical cosmology

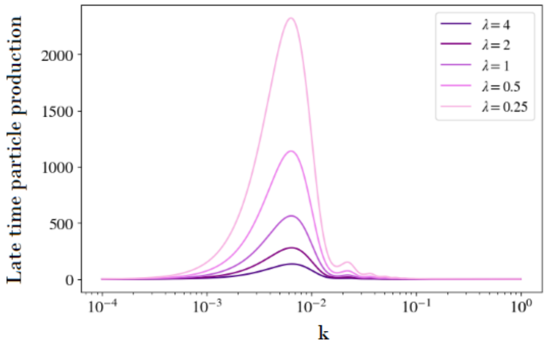

FIG. 8: Late time particle production spectrum for different polymer scales in semiclassical cosmology

Notably, we use the Gaussian ansatz for the matter state because it is simple and enables inexpensive computations. We also determined that for QFTCB at least, it captures the same physics as a more general evolution that the matter can evolve to a non-Gaussian state in. For SG, however, using this general evolution (which needs a large number of modes to evolve the geometry via backreaction) requires huge computational power.

Future directions of exploration include identifying the physical mechanism that selects the mode at which the spectrum peaks and investigating how our results may translate into cosmological observations. A more fundamental quantum cosmological model may be required for both. Other avenues of exploration include generalizations of the current model by incorporating the cosmological constant, anisotropies, and scalar field mass. Relatedly, one may also use matter with nonzero spin to investigate the cosmological abundance of particles for each spin type.

Acknowledgements MS is supported by the FDC award at Centre College. IJ is supported by NSERC.

---

[1] R. M. Wald, *General Relativity* (Chicago Univ. Pr., Chicago, USA, 1984).
[2] H. Halvorson, Studies in History and Philosophy of Science Part B: Studies in History and Philosophy of Modern Physics **35**, 45 (2004).
[3] A. Corichi, T. Vukašinac, and J. A. Zapata, Phys. Rev. D **76**, 044016 (2007).
[4] N. D. Birrell and P. C. W. Davies, *Quantum Fields in Curved Space*, Cambridge Monographs on Mathematical Physics (Cambridge University Press, 1982).
[5] L. Paker and D. Toms, *Quantum Field Theory in Curved Spacetime* (Cambridge University Press, Cambridge, UK, 2009).
[6] E. W. Kolb and A. J. Long, Rev. Mod. Phys. **96**, 045005 (2024).
[7] S. W. Hawking, Commun. Math. Phys. **43**, 199 (1975).
[8] B.-L. B. Hu and E. Verdaguer, *Semiclassical and Stochastic Gravity: Quantum Field Effects on Curved Spacetime*, Cambridge Monographs on Mathematical Physics (Cambridge University Press, 2020).
[9] V. Husain and S. Singh, Phys. Rev. D **99**, 086018 (2019).
[10] V. Husain and S. Singh, Phys. Rev. D **104**, 124048 (2021).
[11] V. Husain and M. Muzammil, Phys. Rev. D **109**, 044063 (2024).
[12] C. Isham, *Structural issues in quantum gravity* (1995), gr-qc/9510063.
[13] C. Kiefer, *Quantum Gravity* (Oxford University Press

UK, 2004).
[14] S. Carlip, D.-W. Chiou, W.-T. Ni, and R. Woodard, International Journal of Modern Physics D **24**, 1530028 (2015).
[15] A. Ashtekar and J. Lewandowski, Classical and Quantum Gravity **21**, R53 (2004).
[16] A. Ashtekar and E. Bianchi, Reports on Progress in Physics **84**, 042001 (2021), ISSN 1361-6633.
[17] A. Ashtekar, T. Pawlowski, and P. Singh, Phys. Rev. Lett. **96**, 141301 (2006).
[18] A. Ashtekar and P. Singh, Classical and Quantum Gravity **28**, 213001 (2011).
[19] V. Taveras, Phys. Rev. D **78**, 064072 (2008).
[20] C. Rovelli and E. Wilson-Ewing, Phys. Rev. D **90**, 023538 (2014).
[21] E. Giovannetti, G. Barca, F. Mandini, and G. Montani, Universe **8**, 302 (2022), ISSN 2218-1997.
[22] M. Saeed and V. Husain, Phys. Rev. D **110**, 103504 (2024).
[23] M. Novello and S. P. Bergliaffa, Physics Reports **463**, 127 (2008), ISSN 0370-1573.
[24] J. Mielczarek, M. Kamionka, A. Kurek, and M. Szydlowski, Journal of Cosmology and Astroparticle Physics **2010**, 004–004 (2010), ISSN 1475-7516.
[25] J. Grain, A. Barrau, T. Cailleteau, and J. Mielczarek, Physical Review D **82** (2010), ISSN 1550-2368.
[26] M. Lilley, L. Lorenz, and S. Clesse, Journal of Cosmology and Astroparticle Physics **2011**, 004–004 (2011), ISSN 1475-7516.
[27] I. Agullo, D. Kranas, and V. Sreenath, General Relativity and Gravitation **53** (2021), ISSN 1572-9532.
[28] C. Li, R. H. Brandenberger, and Y.-K. E. Cheung, Physical Review D **90** (2014), ISSN 1550-2368.
[29] L. J. Garay, M. Martín-Benito, and E. Martín-Martínez, Physical Review D **89** (2014), ISSN 1550-2368.
[30] G. Mahajan and T. Padmanabhan, General Relativity and Gravitation **40**, 661–708 (2007), ISSN 1572-9532.
[31] G. Mahajan and T. Padmanabhan, General Relativity and Gravitation **40**, 709–747 (2007), ISSN 1572-9532.